# Acoustic Tracking of Aircraft Using a Circular Microphone Array Sensor

Ines Hafizovic
University of Oslo/Squarehead Technology AS
Oslo, Norway
Email: ines@sqhead.com

Carl-Inge Colombo Nilsen
University of Oslo
Oslo, Norway
Email: carlingn@ifi.uio.no

Morgan Kjølerbakken
Squarehead Technology AS
Oslo, Norway
Email: morgan@sqhead.com

***Abstract*—Runway Incursion Avoidance Systems (RIAS) are vital parts in the prevention of runway accidents at airports. Such systems depend on the accurate positioning of aircraft and ground vehicles. Today, RADAR is the predominant method, but a RADAR based system might be both impractical and too expensive for small airports. Additionally, the redundancy of several independent systems is sought after even at large airports. We investigate the application of a low-cost circular microphone array solution for acoustic detection and tracking of aircraft. The shape of the array yields $360^\circ$ coverage with equal characteristics in all directions. An algorithm based on sweeps performed with the Capon adaptive beamformer followed by peak detection and thresholding is implemented for real time use. The performance of the system is tested at Evenes airport in Norway.**

## I. Introduction

Runway incursions are commonplace at airports and can have tragic outcomes such as the 2001 Milan airport collision, or the ground collision at Tenerife airport in 1977. On-ground security at airports is primarily based on information from surface movement radars. Radar based systems for on-ground traffic routing and control are complex and costly to implement, especially for smaller airports. At many smaller airports security relies often on communication with the tower. Increased traffic, cancellations, and delays, together with the lack of visibility safeguards, are posing a constant threat to the on-ground safety. Major security gaps can be caused by language barriers, unfamiliarity with the airport, low visibility of surface movements from the tower, and more.

Previously suggested cost-effective solutions for tracking and monitoring of aircraft on the ground are based on visual tracking. An airport ground surveillance system based on video cameras is proposed in [1] and [2]. The use of infrared cameras has also been suggested,e.g. in [3]. Camera-based solutions are good supplements to e.g. surface radars, which can have blind spots. However, these solutions come with weather limitations. Low visibility can cause poor detection with video cameras, and occlusion can cause false detections with infrared cameras.

Acoustic tracking has the potential to overcome the above mentioned limitations. Acoustic detection and tracking of aircraft has been proposed earlier, both with traditional pressure microphones, and with three dimensional acoustic probes. In [4], a 3D sound probe system is tested in real environments on helicopter movements, and in [5], fast moving aircraft flying at low heights are localized using microphones. However, main focus in most proposals is tracking and detection of flying aircraft. Unlike previous proposals, we use a two dimensional circular microphone array placed parallel to the runway to detect presence of aircraft. We use a multi-ring, wideband, circular array combined with a high resolution beamforming algorithm, the Capon beamformer, for real time detection of aircraft within array's coverage area. With known coordinates of the sensor array position, the detected angle is translated to aircraft's coordinates which are sent to the airport's on-ground security and alarm system. Outputs from several sensors along the runway can be combined for triangulation purposes and thus cover large areas. The Capon beamformer has previously been suggested for acoustic target detection in e.g. [6], but with distributed sensors, and for general moving targets. Our proposal is designed for the special case of aircraft tracking on runways.

The applied acoustic sensor is comprised of 105 digital MEMS microphones to ensure redundancy. In this paper we present the performance of such a sensor for the potential use as part of a runway incursion avoidance system (RIAS). Tests in a real environment (on an active air field) show no failure in detections of aircraft with their engines on, and a detection accuracy within one aircraft length. The results presented here are quite promising, but further tests need to be done to confirm the performance and robustness under different weather conditions.

In section II we cover the necessary theoretical background, which is the principles of beamforming and the Capon adaptive beamformer. In section III we present the measurements taken at Evenes airport as well as some results of the tracking algorithm. In section IV we discuss the results.

## II. Theoretical Background

### A. Sensor Arrays and Beamforming

When multiple sensors are arranged in a grid, a sensor array is formed. Arrays of sensors can be made highly directive and have the attractive feature of electronic steering, i.e. by processing the data from array elements, an array can enhance signals coming from directions of interest and suppress noise coming from other directions. Sensor arrays are commonly used in applications like radar, sonar, ultrasound imaging, and microphone arrays for speech applications. We will be dealing

978-1-4244-5128-9/10/$26.00 ©2010 IEEE

with a two dimensional microphone array sensor, comprised of low-cost, omni-directional microphones.

Just as a single microphone, each microphone in the array samples sound in time. When time sampled signals from multiple microphones placed at different locations are combined, we sample the same sound in space as well. To avoid strong contributions from interferers outside the look direction, the array must satisfy the spatial sampling criterion saying that the distance between elements must be smaller than half the wavelength of the highest frequency received by the array. If this is not satisfied, the spatial aliasing will occur and manifest itself as *grating lobes* in the beampattern.

The outputs of multiple sensors (microphones) can be combined in different ways to form one or several array outputs. An algorithm used to combine multiple sensor outputs into one is generally called a beamformer. A simple, but a robust beamformer is the delay-and-sum beamformer.

For an array comprised of M elements, the signal vector for time sample $n$ can be denoted as

$$\vec{x_n} = [x_0[n], ..., x_{M-1}[n]]^T \tag{1}$$

For a single frequency $k$, the signal at time sample *n* and for m-*th* sensor is

$$X_{nm}[k] = DFT\{x_m[n]\}_{N_{dft}}, \tag{2}$$

forming a frequency domain data vector:

$$\vec{X}_n[k] = \left[X_{n0}[k], \cdots, X_{n(M-1)}[k]\right]^T \tag{3}$$

The output of a delay-and-sum beamformer applied to an M-element array with sensor positions $\vec{p}_m, m = 0, 1, ..., M-1$, focused on a source located at a point $\vec{p}_s$, can be now written as:

$$Y_n[k] = \sum_{m=0}^{M-1} w_m[k] X_{nm}[k]. \tag{4}$$

Here, $w_m[k]$ is a weighting coefficient for m-*th* sensor element, and is a combination of sensor amplitude weighting $g[k]$ and a delay corresponding to a chosen look direction and frequency $k$,

$$w_m[k] = \sum_{m=0}^{M-1} g_m[k] e^{\frac{j2\pi f_s k \|\vec{p}_m - \vec{r}_i\|}{cN_{dft}}} \tag{5}$$

In further discussion we will assume that

$$\sum_{m=0}^{M-1} w_m = 1, \tag{6}$$

meaning that any signal coming from the steering direction $\vec{p}_s$ will be unaffected by the array. The vector of exponentials in (5) is in the literature denoted as $\vec{v}$ and often called the *steering vector*. Throughout this document, we will use the following definition:

$$\vec{v}[k] = \left[e^{\frac{j2\pi f_s k \|\vec{p}_0 - \vec{p}_s\|}{cN_{dft}}} \cdots e^{\frac{j2\pi f_s k \|\vec{p}_{M-1} - \vec{p}_s\|}{cN_{dft}}}\right]^T. \tag{7}$$

When the signal from element $m$ is delayed by $|\vec{p}_m - \vec{p}_s| / c$ seconds, signals coming from the source at $\vec{p}_s$ are temporally aligned. Signals coming from other directions will generally be out of phase. Noise that is uncorrelated from element to element (e.g. sensor-induced noise, wind noise) is always out of phase, independently of the array's look direction. By summation across elements, we can therefore reduce the sensor-induced noise and effectively filter out sources from other directions than $\vec{p}_s$ , i.e. the look direction.

### *B. Capon Beamforming*

The Capon beamformer was proposed for the first time in [7]. Compared to the delay-and-sum beamformer, the Capon beamformer is a high resolution method. While the delay-and-sum beamformer has fixed weights $\vec{w}$, the weights of the Capon beamformer are adapted to best fit the actual signal environment. The Capon beamformer satisfies the optimality criterion of Minimum Variance Distortionless Response (MVDR), which means that it finds the weights $w_m[k]$ that minimize the variance $E\{|Y_n[k]|^2\}$ of the output $Y_n[k]$ in (4) under the constraint that any signal coming from a predefined direction of interest remains unaffected. This constraint is necessary e.g. to ensure a non-trivial solution $\vec{w} \neq \vec{0}$.
Adaptive methods like the Capon beamformer generally provide better resolution than conventional methods like delay-and-sum. This is demonstrated in Fig. 1 for a two-source scenario and a uniformly spaced linear array (i.e. not the same array as used in this paper). An advantage of the adaptive methods is that a small array (in terms of aperture) combined with an adaptive method can provide the same resolution as a much larger array in combination with a delay-and-sum beamformer. The Capon beamformer is a non-parametric adaptive method, i.e. it does not require other a priori assumptions than no presence of correlated sources. The spectra of a few representative aircraft and the correlation between them is shown in next section, in Fig. 7. A disadvantage of adaptive methods is that they are based on unknown signal statistics that must be estimated from received data. This can make the beamformer both computationally demanding and numerically unstable. A thorough guide to overcoming most of these issues surrounding Capon beamforming can be found in e.g. [8].

The adaptive weights of the Capon beamformer are found by solving the following optimization problem:

$$\min_{\vec{w}} P(\vec{w}) \text{ subject to } \vec{w}^H \vec{v} = 1 \tag{8}$$

where $P(\vec{w})$ is the output power given by

$$\begin{aligned} P(\vec{w}) &= \frac{1}{N} \sum_{n=0}^{N} |Y_n[k]|^2 \\ &= \frac{1}{N} \sum_{n=0}^{N} (\vec{w}[k]^H \vec{X_n}[k])(\vec{w}[k]^H \vec{X_n}[k])^H \\ &= \vec{w}[k]^H \mathbf{R}[k] \vec{w}[k]. \end{aligned} \tag{9}$$

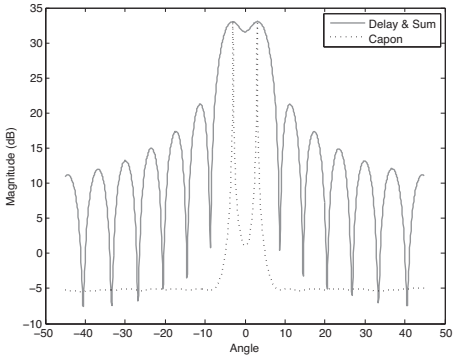


Fig. 1. Resolution of the delay-and-sum beamformer compared to resolution of the Capon beamformer for the linear array.

Fig. 2. The sensor array at the test site.

The matrix $\mathbf{R}$ is the covariance matrix, which equals:

$$\mathbf{R}[k] = \frac{1}{N}\sum_{n=0}^{N} \vec{X}_n[k]\vec{X}_n[k]^H. \quad (10)$$

The optimum weights, $\vec{w}_{CAP}$, are found by solving the optimization problem in (8), and are given by

$$\vec{w}_{CAP}[k] = \frac{\mathbf{R}[k]^{-1}\vec{v}[k]}{\vec{v}[k]^H\mathbf{R}[k]^{-1}\vec{v}[k]}. \quad (11)$$

Inserting these weights into the power expression (9), the output power of the Capon beamformer becomes

$$P_{CAP}[k] = \frac{1}{\vec{v}[k]^H\mathbf{R}[k]^{-1}\vec{v}[k]}. \quad (12)$$

Since the Capon beamformer requires inversion of the covariance matrix, the method can become numerically unstable. Several measures can be taken to ensure stability, like using a larger number of time samples than the number of sensor elements in the array, i.e. $N > M$ in (10). The covariance matrix can be made invertible by adding a scaled identity matrix to it before the inversion,[9]. This procedure is known as diagonal loading, and can for instance be done adaptively as

$$\hat{\mathbf{R}}^{-1} = (\mathbf{R} + \frac{\delta}{M} trace\{\mathbf{R}\}\mathbf{I})^{-1}, \quad (13)$$

where $\delta$ is a user defined constant.

## III. Measurements

### A. Tracking Sensor

The microphone array inside the sensor shown in Fig. 2 is a circular array of four concentric circles, and in total 105 MEMS microphones. This is the inner part of the array described in [10]. The inter-circle distances are exponential for a broader frequency response, as detailed in [11]. The shown array is suitable for spatial processing of frequencies up to 3.5kHz. In these tests we use a narrow-band approach, where we extract individual frequency bins from a broadband signal. The number of processed bins and their frequencies can vary, and several bins can be combined for wideband detection purposes. Only 45 of the 105 microphones are processed per bin in the narrow-band approch. The geometry of the array elements for which the results are shown, can be seen in Fig. 3.

Data acquisition and processing is done as illustrated in Fig. 4. The processing chain is as follows:

1) Data are acquired by the microphones which are sampled and filtered on an FPGA-based system.
2) The acquired data are transmitted to a computer and placed in a buffer.
3) Data are taken from the buffer and transformed to the frequency domain using an FFT. Frequency coefficients for all sensors and from several sequential FFTs are arranged in vectors and used to form a covariance matrix.
4) The Capon beamformer outputs are formed for the following $L$ spherical coordinates $\theta = \pi/2, \phi_l = \frac{2\pi}{L}l, l = 0, 1, \cdots, L-1$. This process results in an $L$-element vector which we will refer to as a *beamformer sweep* in which the elements correspond to the magnitude of the signal arriving from direction $(\theta, \phi) = \left(\frac{\pi}{2}, \phi_l\right), l = 0, 1, \cdots, L-1$.
5) The peak values of the beamformer sweep are found, along with their corresponding angles.
6) Peak values that are under a certain threshold are discarded.
7) The angles and values of the remaining peaks are transmitted from the array to a central system, where local angles can be translated into longitude and latitude.

### B. Tests

The primary goal of the in situ test was to confirm the following assumptions:

- A horizontally placed array with normal axis facing upwards can be used for aircraft noise field sampling.
- The array can detect aircraft within a range of 340m (the distance corresponding to 1s sound travel time).
- The Capon beamformer is applicable for aircraft detection.
  - Detection and transmission of results can be done in real time.

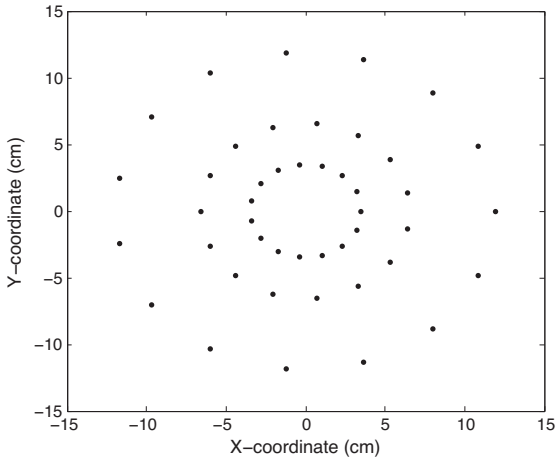


Fig. 3. The geometry of the applied microphone array.

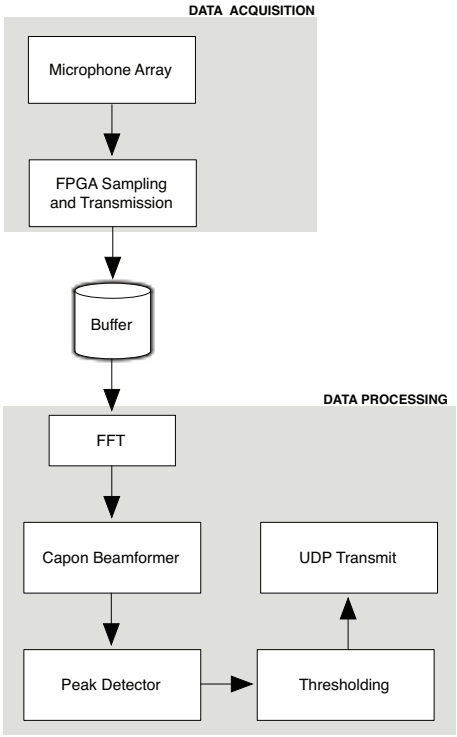


Fig. 4. Flowchart of the tracking system.

- Detection can be done for different types of aircraft with the same parameters.
- Detection can be done with good accuracy.
- No false detections.

An overview picture of the test site with the sensor array placed between two runways is shown in Fig. 5. The tests were performed over three days, under windy conditions, with a maximal wind speed of 15m/s. The array was mounted 2-2.5m above the ground with direct line of sight to the aircraft, as shown in Fig. 2. We monitored slow taxying (area 1 and 2 in Fig. 5), and landings and take offs (at the upper runway, area 3 in Fig 5). This was done for all scheduled flights at these runways during the test period. The two dominating types of aircraft were Boeing 737 and Dash-8.

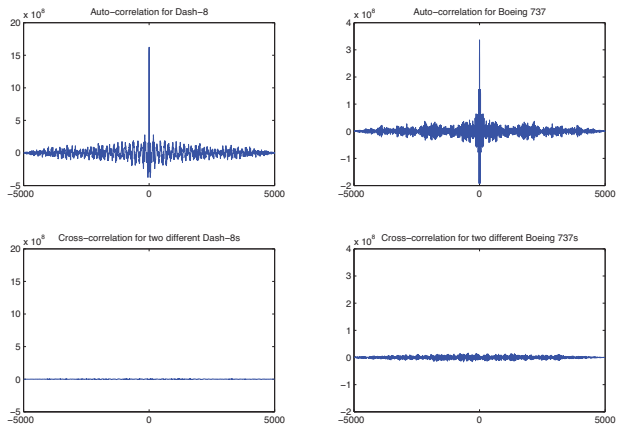


Fig. 7. Auto- and cross-correlation for Boeing 737 and Dash 8 airplanes.

### C. Spectral Characteristics of Airplane Noise

The power spectra for the two airplanes of interest, i.e. Boeing 737 and Dash-8, are shown in Fig 6. These show that frequency bands below 2kHz contain more energy than the higher bands. Based on these observations, we chose an average of two frequency coefficients: $f_0 = 1291$ Hz and $f_2 = 1808$ Hz for our Capon tracker.

The auto- and cross-correlations for the same airplanes are shown in Fig. 7. It is clear from these plots that the sound coming from different airplanes will not be correlated, meaning that the previously stated assumption for Capon robustness is fulfilled.

### D. Calibration

Ahead of the measurements, a calibration of the sensor was done in situ. The output of the array was adjusted to match the sound pressure levels registered with a sound level meter. The threshold for detections was adjusted to exclude random fluctuations in background noise levels (max. 73dBA due to wind, average 60dBA). The sound intensity measured with a sound level meter at the position of the sensor array with airplanes passing in at a distance of 50m was max. 87dBA and min. 80dBA. The airplane noise intensity varied with the airplane's speed (engine load).

After the array sensor was rigged, as in Fig. 5, its longitude and latitude were registered. Assuming that the airplanes are using the middle of the runway, relative angles between the sensor and the aircraft translate directly into absolute coordinates used in the RIAS. In order to assess the accuracy of detections we placed physical markers at $45°$, $90°$, $135°$, and $270°$ relative to the array, as indicated with yellow labels in Fig. 5. The output of the tracker was matched with visual observations of airplanes passing the markers.

In the presented measurements, the angle sweeps (aircraft

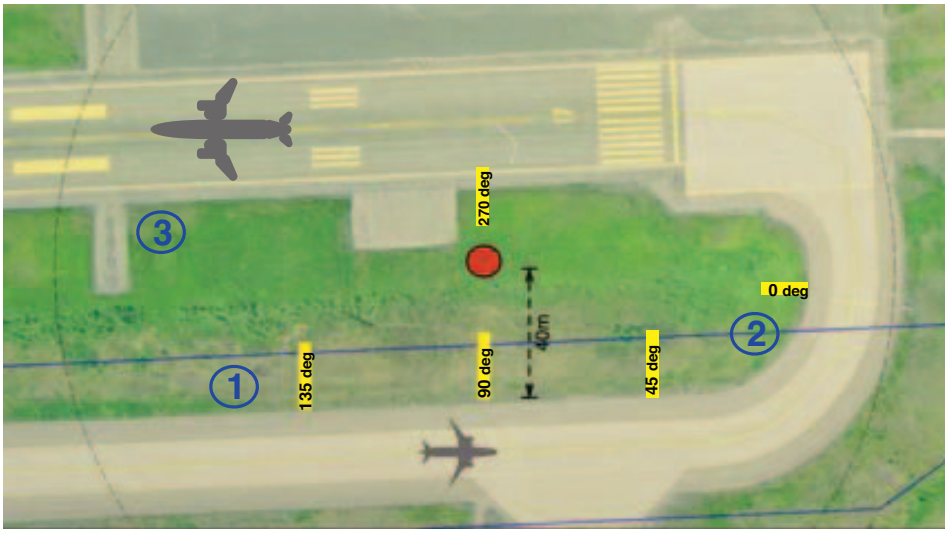


Fig. 5. Test site with sensor array.

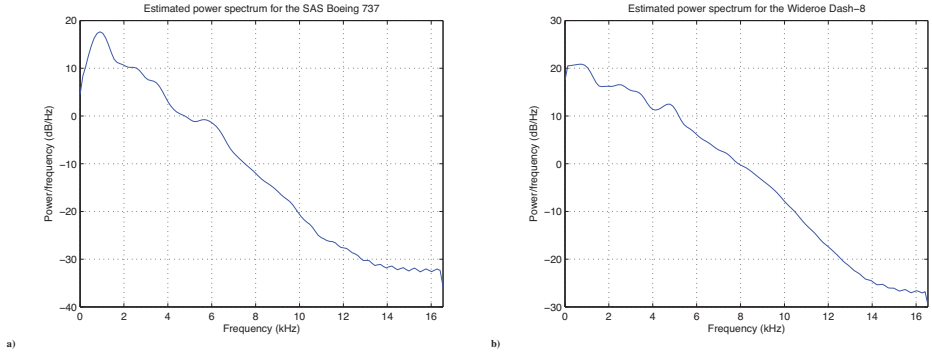


Fig. 6. Power spectra of **a)** SAS Boeing 737 and **b)** Widerøe Dash-8.

searches) are performed at least 4 times a second. Meaning that the positioning accuracy is 250ms, or 3.5m for an airplane taxying at 50km/h.

### *E. Positioning Results*

In this section we present results for the dominating types of aircraft that we monitored during three consecutive days of measurements. We present a few representative results, with a general observation that the results for a given type of airplane show similar trends under similar conditions.

The output of the tracker for an SAS Boeing 737 during taxying on the lower runway (1 in Fig. 5) before takeoff is shown in Fig. 10. All the angles used in Fig. 10 correspond to the angles in Fig. 5.

In subfigure 10**a)** we see the calculated beamformer sweeps as a function of time. The main source is clearly visible, moving across angles as time progresses, with a small ambiguity present at an angular distance of $180°$. This was experimentally confirmed to be caused by diffraction around the spherical array housing. The tracking algorithm does not report this diffraction source, due to the thresholding step. The main source is seen as progressing from $150°$ to $0°$, which corresponds to movement from point 1 to point 2 in Fig. 5.

In subfigure 10**b)** we see the angle corresponding to the maximum value of each beamformer sweep from Fig. 10**a)** as a function of time. The squares mark whenever the detected angle indicates movement in the wrong direction. The majority of detection fluctuations occur after the above mentioned drop-off in magnitude, i.e. at angles lower than $45°$. From Fig. 5, we see that this corresponds to a region in which the rear part of the aircraft is facing the array. These are small fluctuations, within the length of the airplane in question. For an airplane 50m away from the array, maximal detection ambiguity is 7m. These fluctuations are only occurring when the rear of a slowly taxying airplane is facing the array, which indicates that airplane engines are not isotropic sources.

In subfigure 10**c)** we see the magnitude of the signal received by the array as a function of time. Additionally, we show the *beamformer dynamic range*, which we define as the difference between the maximum peak and the background noise level of a single beamformer sweep. The peak magnitude

occurs after about 14 seconds, which we see from Fig. 10**b)** that corresponds to an angle of $70°$. A sharp drop-off in magnitude occurs after about 17 seconds, corresponding to the aircraft being at an angle of $50°$, shown in Fig. 10**b)**. Note how the dynamic range decreases at a lower rate than the magnitude. This means that when the peak representing the aircraft decreases in magnitude, so does the noise floor, retaining the initial dynamic range. This indicates that the noise floor mainly consists of the aircraft-induced noise, e.g. multipath propagation and sidelobe contributions. However, peak detection is not severely affected by the magnitude drop, as long as the noise floor falls in the same manner. An SPL threshold rejecting sources less than 5-10dB above the background noise level would suffice to detect this aircraft.

The output of the tracker for a Widerøe Dash-8 during taxying before takeoff is shown in Fig. 11. Unlike the SAS Boeing 737, this plane used the upper runway when taxying. In subfigure 11**a)** we see the calculated beamformer sweeps as a function of time. Again, the main source is clearly visible with an ambiguity at an angular distance of $180°$. The main source is seen as progressing from $200°$ to $360°$, which corresponds to movement from point 3 to point 2 in Fig. 5.

In subfigure 11**b)** we see the angle corresponding to the maximum value of each beamformer sweep from Fig. 11 **a)** as a function of time. Unlike the Boeing 737, the Dash 8 was not seen moving in the wrong direction by the beamformer. In addition, the drop in magnitude, as shown in subfigure 11**c)**, is somewhat lower than for the Boeing 737 in Fig. 10**c)**. An SPL threshold rejecting sources less than 10-15 dB above the background noise level would suffice to detect this aircraft.

### *F. Potential Issues*

It is important to have in mind that the sound intensity falls with 6dB for each doubling of the distance from a source in free field, and that there is an additional attenuation from atmospheric absorption whose value is a function of frequency, and depends on both temperature and relative humidity, as shown in table in Fig. 8. For 1kHz and 20°C for instance, this attenuation is 0.0042dB/m at 100% humidity, and 0.018dB at 10%. Loss for higher frequencies is even higher, e.g. attenuation at 5kHz over a 200m path length can reach 22dB. These numbers illustrate that the range of an acoustic sensor will depend on the choice of detection frequency and weather conditions.

In addition, the speed of sound is influenced by air temperature, and higher temperature corresponds to an increase in sound speed. This relationship is given by $c = 20.06\sqrt{T}$, where $T$ is the absolute temperature in degrees Kelvin. Thermal gradient will cause sound diffraction, and normal thermal gradients in air correspond to a temperature decrease with increased elevation. Such conditions diffract air upward, towards the cooler layers, so that apparent direction of propagation is elevated. For typical outdoors conditions, the sound can be diffracted with approximately 5 degrees over 200m, corresponding to a 17.5m shift in elevation. This indicates that an acoustic array may need to sweep the elevation angle as well.

***Relative Humidity %***

| *Frequency (kHz)* | **10** | **20** | **30** | **40** | **50** | **60** | **70** | **80** | **90** |
|---|---|---|---|---|---|---|---|---|---|
| **1** | 14 | 6.5 | 5 | 4.7 | 4.7 | 4.8 | 5 | 5.1 | 5.3 |
| **1.25** | 21 | 9.4 | 6.7 | 5.9 | 5.7 | 5.7 | 5.9 | 6.1 | 6.3 |
| **1.6** | 32 | 14 | 9.8 | 8.1 | 7.5 | 7.2 | 7.2 | 7.4 | 7.5 |
| **2** | 45 | 22 | 14 | 11 | 9.9 | 9.3 | 9 | 9 | 9.1 |
| **2.5** | 63 | 32 | 21 | 16 | 14 | 12 | 12 | 11 | 11 |
| **3.15** | 85 | 49 | 32 | 24 | 20 | 17 | 16 | 15 | 15 |
| **4** | 110 | 75 | 49 | 36 | 30 | 26 | 23 | 21 | 20 |
| **5** | 130 | 110 | 74 | 55 | 44 | 38 | 33 | 31 | 28 |
| **6.3** | 160 | 160 | 110 | 84 | 68 | 57 | 50 | 45 | 42 |

Fig. 8. Attenuation of sound in air (dB/km), at 20°C.

The last mechanism contributing to potential detection errors is wind. The effect of wind is twofold. Wind speed near the ground is normally less than higher up. The sound waves propagating against the wind are diffracted upward, while the sound propagating in the same direction as the wind is diffracted downward. Additionally, sound propagates across greater distances with the wind than against the wind, and the registered effect is a modulated sound intensity. Crosswinds will shift the axis of propagation towards that of the wind direction. This is the potentially largest problem for aircraft detection, because it will cause the sound waves to appear as they are coming wrong directions. A worst case scenario for this distortion can be considered by assuming that wind speed $v_w$ will be below 25m/s, since higher wind speeds usually prevent normal air traffic. An aircraft located $40 < d < 340$ meters from the array and at an angle where a line through the array and aircraft is normal to the direction of the wind, will experience maximum sound displacement. This displacement in meters is equal to $\delta = \frac{d}{340} v_w$, which for a wind speed of 25m/s yields $3 \leq \delta \leq 25$ meters. This is, at most, slightly larger than the length of a Dash 8, but shorter than the length of a Boeing 737. A graph presenting the detection displacement for any combination of distance and wind speed can be found in Fig. 9. More on outdoor sound propagation can be found in [12], [13].

From the results in this paper, we have seen that normal ambient noise (such as wind and remote traffic), as well as multipath propagation etc., does not lead to false detections or detection failures with the proposed method. It is, however, easy to imagine that sporadic noise can have the ability to cause false detections. Some examples worth considering are:

- Thunder.
- Sound from birds.
- Sounds from nearby construction sites, such as explosions and heavy machinery.

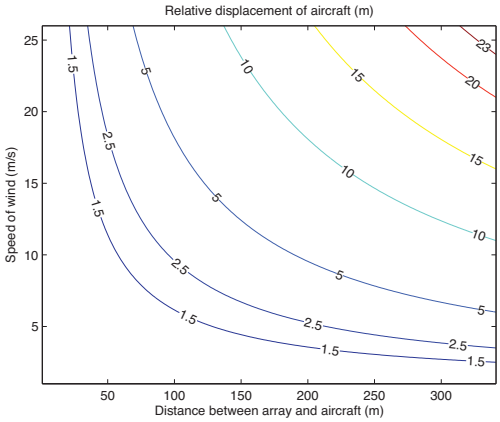


Fig. 9. Apparent displacement of airplane due to wind

Although all of the above are examples of signals that can contain the frequencies necessary to trigger false detections, there is one property that they do not share with aircraft engine noise; they are impulse-like and not stationary. We can utilize this by examining signal properties in the time domain as well as the spatial domain for all detected sources. We can define certain criteria that the time domain measurements of each peak in the beamformer sweep must satisfy to qualify as a source; for instance that it must sustain a certain magnitude for a certain duration, or that its spectrum must be similar to those of Fig. 6.

## IV. Discussion

We implemented and tested a microphone array as a tracking sensor for a runway incursion avoidance system. The Capon based tracker, combined with the proposed sensor proved to be suited for aircraft tracking under the described test conditions. The acoustic sensor system performed very well for Boeing 737 and Dash-8 airplane types, under taxying, landing, and take-offs. The thresholding in the tracking algorithm ensured zero false detections. We observed small fluctuations (max. 7m) in positioning of Boeing 737 when the rear part of the airplane was facing the array. The tests indicate that the fluctuations are caused either by the directivity pattern of the engines, or some physical effects occurring at the rear (e.g. reflections from the fuselage). This has to be confirmed by further investigation of different aircraft engines in different orientations. The detection accuracy, for an update rate of 4 times/s and distances 50-100m, was always within an airplane length. To confirm the accuracy for larger distances, acoustic tracker results must be compared with e.g. radar data. The spatial signal to background noise ratio has proven to be satisfactory, even at large distances and under windy conditions. The acoustic sensor was able to register aircraft several hundreds meters away from the sensor. However, due to the retardation, these data are not considered as reliable for RIAS application, where an accuracy of max. 1 second is required.

The proposed system is cost effective and has potential as a part of a runway incursion avoidance system. Multiple sensors can easily be combined for triangulation. The flexibility of the proposed solutions should also be pointed out. Signal processing of array data can be done in many ways without hardware adaptations and a part of future work should be an investigation of other adaptive methods. Acoustic array data can also be used for other purposes than tracking, possibly aircraft type recognition. The long-term reliability of an acoustic sensor under various weather conditions (presence of temperature gradients, storms, rain falls, extreme temperature, and more) should also be documented.

## Acknowledgment

The authors would like to thank Unified Messaging Systems AS (Kjell Harald Heen, Tom Muggerud, Håkon Frøyset, and Morten Helvig) for initializing this project, taking a part in fieldwork, and providing the communication with RIAS. We would also like to thank our team at Squarehead Technology AS for programming help (Andreas Holm and Johannes Alming Daleng), hardware design (Tor Anstein Olsen), and the construction of the sensor (Audun Hovslien).

## References

[1] J. Besada, J. M. Molina, J. Garcia, A. Berlanga, and J. Portillo, "Aircraft identification integrated into an airport surface surveillance video system," *Machine Vision and Applications, Vol 15, No. 3, pp. 164-171*, 2004.

[2] N. Pavlidou, N. Grammalidis, K. Dimitropoulos, D. Simitopoulos, A. Gilbert, E. Piazza, C. Herrlich, R. Heidger, and M. Strintzis, "Using intelligent digital cameras to monitor aerodrome surface traffic," *IEEE Journal of Intelligent Systems*, 2005.

[3] C. F. R. Castaldo and A. Smith, "Evaluation of flir/ir camera technology for airport surface surveillance," *10th Annual International AeroSense Symposium, Orlando*, 1996.

[4] T. Basten, H. de Bree, and E. Tijs, "Localization and tracking of aircraft with ground based 3d sound probes," *33rd European Rotorcraft Forum (ERF), Kazan, Russia*, 2007.

[5] F. Dommermuth, "A simple procedure for tracking fast maneuvering aircraft using spatially distributed acoustic sensors," *Journal of the Acoustical Society of America, Vol 82, No. 4, pp. 1418-1424*, 1987.

[6] M. R. Azimi-Sadjadi and N. R. A. Pezeshki, "Wideband doa estimation algorithms for multiple moving sources using unattended acoustic sensors," *IEEE Transactions on Aerospace and Electronic Systems, Vol. 44, No. 4, pp. 1585-1599*, 2008.

[7] J. Capon, "High-resolution frequency-wavenumber spectrum analysis," *Proc. IEEE, Vol.57, No. 8, pp.1408-1418*, 1969.

[8] H. V. Trees, *Optimum Array Processing*. Wiley-Interscience, 2002.

[9] B. D. Carlson, "Covariance matrix estimation errors and diagonal loading in adaptive arrays," *IEEE Transactions on Aerospace and Electronic Systems, Vol. 24, No. 4, pp. 397-401*, 1988.

[10] I. Hafizovic, M. Kjølerbakken, and V. Jahr, "System configuration for high quality audio capturing in a large microphone array," *AES 31st International Conference, New Directions in High Resolution Audio*, 2007.

[11] A. Ishimarur, "Theory of unequally-spaced arrays," *Antennas and Propagation, IEEE Transactions on [legacy, pre - 1988], vol. 10, Iss.6, pp. 691-702*, 1962.

[12] K. Rasmussen, "Outdoor sound propagation under the influence of wind and temperature gradients," *Journal of Sound and Vibration, Vol. 104, No. 2, pp. 321-335*, 1986.

[13] M. Diamond, "Cross wind effect on sound propagation," *Journal of Applied Meteorology, Vol. 3, pp. 208-210*, 1964.

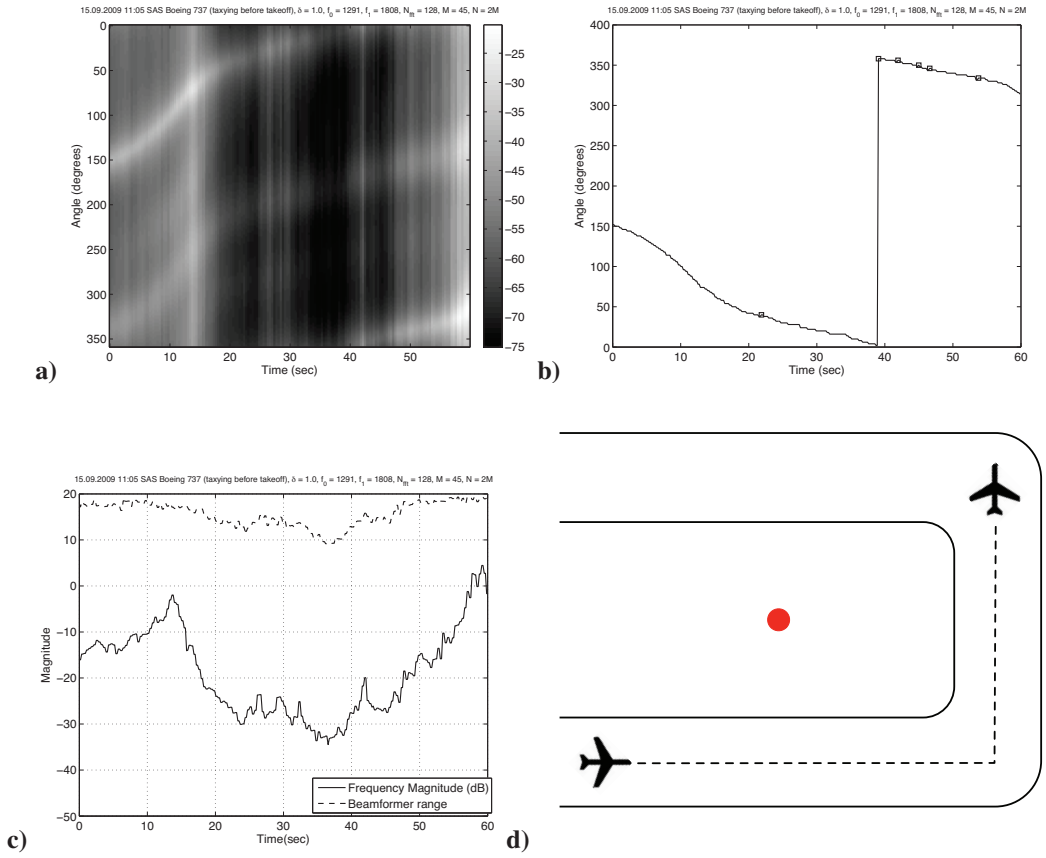


Fig. 10. Measurements of a SAS Boeing 737 while taxying before takeoff. Taxying occurs on the lower runway of 5.

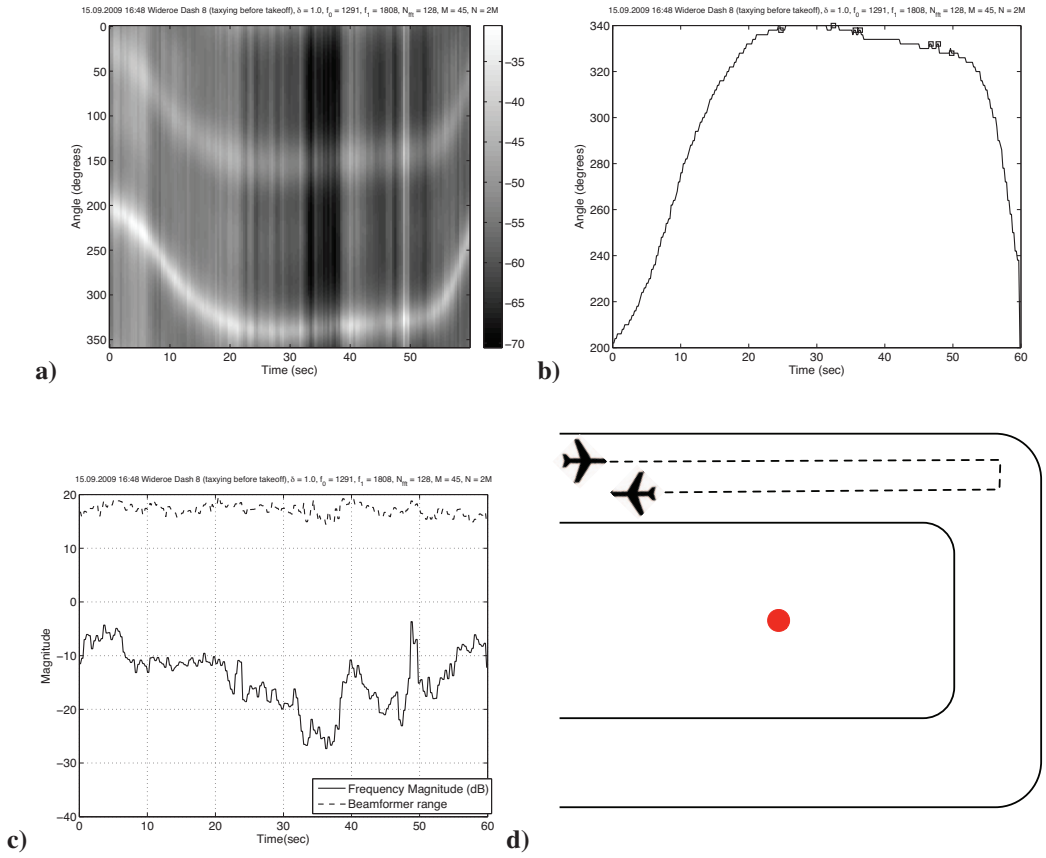


Fig. 11. Measurements of a Widerøe Dash 8 while taxying before takeoff and while taking off. Both taxying and takeoff takes place on the upper runway of Fig. 5.